Available online at www.sciencedirect.com

ScienceDirect

Green Energy & Environment 1 (2016) 258−265

www.keaipublishing.com/gee

Research paper

Simultaneous measurement of CO_2 sorption and swelling of phosphate-based ionic liquid

Junfeng Wang [a,*], Camille Petit [d], Xiangping Zhang [a], Ah-Hyung Alissa Park [b,c,**]

[a] National Key Laboratory of Biochemical Engineering, Institute of Process Engineering, Chinese Academy of Sciences, Beijing 100190, PR China
[b] Department of Earth & Environmental Engineering, Lenfest Center for Sustainable Energy, Columbia University, 500 W. 120th Street, New York, NY 10027, USA
[c] Department of Chemical Engineering, Lenfest Center for Sustainable Energy, Columbia University, 500 W. 120th Street, New York, NY 10027, USA
[d] Department of Chemical Engineering, Imperial College London, South Kensington Campus, London SW7 2AZ, UK

Received 29 September 2016; revised 15 November 2016; accepted 15 November 2016
Available online 25 November 2016

Abstract

The development of alternative CO_2 capture solvents such as ionic liquids (ILs) and nanoparticle organic hybrid materials (NOHMs) have provided interesting options for CO_2 capture. In this study, CO_2 interactions with 1,3-dimethylimidazolium dimethylphosphate ([MMIM]DMP), 1-ethyl-3-methylimidazolium dimethylphosphate ([EMIM]DMP) and 1-ethyl-3-methylimidazolium diethylphosphate ([EMIM]DEP) that contain inorganic ester groups based on phosphate, were investigated using ATR FT-IR spectroscopy. CO_2-induced swelling, CO_2 diffusivity and CO_2 capture capacity were simultaneously measured to identify CO_2 capture mechanisms, kinetics and diffusion behaviors as a function of the alkyl chain length of the cation. Henry's law constants of CO_2 were found to be in the range of 4−11 MPa, which is in agreement with those reported in other studies.

Keywords: CO_2 capture; ATR FT-IR spectroscopy; Ionic liquids; Mechanism; Diffusivity

1. Introduction

Carbon capture and storage (CCS) is one of the most difficult environmental problems with unprecedented scale. Capturing CO_2 from large point sources has become a global and urgent issue since the escalating atmospheric concentration of CO_2 is threatening the delicate balance on Earth. The conventional technology to capture CO_2 is chemical absorption using amine-based solvents. While offering fast kinetics and high CO_2 capture capacities, amine scrubbing still faces a number of challenges including a high energy demand, the degradation of the amine, the release of volatile organic compounds, and the risk of equipment corrosion. Room temperature ionic liquids (RTILs) have been considered as promising alternative solvents to address some of these challenges of amine scrubbing [1−4]. RTILs possess many attractive properties, such as non-flammability, high thermal stability, wide electrochemical window, and tunable properties *via* the combination of different cations and anions [5−8]. One of the main reasons to use ILs for CO_2 capture lies in their negligible vapor pressure, which decreases the risk of worker exposure and that of material loss. Additionally, compared to the amine-based reagents, which utilize strong chemical interactions with CO_2 by forming carbamate species, the separation of CO_2 through physical interaction is particularly attractive because the stripping of CO_2 from a RTIL can be operated under much milder conditions thereby reducing the overall operation cost.

Several recent studies have reviewed the main aspects of the use of RTILs for CO_2 capture [9−14]. Cadena et al.

* Corresponding author.
** Corresponding author.
E-mail addresses: junfwang@ipe.ac.cn (J. Wang), ap2622@columbia.edu (A.-H.A. Park).

http://dx.doi.org/10.1016/j.gee.2016.11.004

investigated the effect of anions in alkylimidazolium-based ILs for CO_2 capture *via* experimental and molecular simulation studies. They revealed that the anions play a critical role in interacting with CO_2 because anions containing fluorine exhibit a high affinity toward CO_2 [9]. Anthony et al. observed that [BMIM]Tf_2N exhibited relatively high capacity for CO_2 while [BMIM]BF_4 and [BMIM]PF_6 had lower affinity for CO_2 [10]. Brennecke et al. investigated the effect of anions and cations in imidazolium-based ILs on the solubility of CO_2. Results showed that solubility of CO_2 in [BMIM]-based ILs is strongly dependent on the choice of the anion and increases in the following order: $[NO_3] < [DCA] < [BF_4] \sim [PF_6] < [TfO] < [Tf_2N]$. Additionally, they observed that an increase in the alkyl chain length of the cation increases the CO_2 solubility marginally [11].

Despite these findings, there is still a long path ahead to find suitable material candidates that are competitive, both from economic and technological viewpoints, compared to currently available processes such as the widely used amine-based solvents [15]. Brennecke et al. found that it was difficult to employ the task-specific ILs in industrial applications due to the increasing viscosity after the absorption reaction [8]. Wasserscheid et al. have found that the presence of halogen atoms in typical ionic liquids containing anions (such as $[AlCl_4]^-$, $[PF_6]^-$, $[BF_4]^-$, $[TfO]^-$ or $[Tf_2N]^-$) may cause serious concerns if the hydrolysis stability of the anion is poor (*e.g.* for $[AlCl_4]^-$ and $[PF_6]^-$) or if a thermal treatment of spent ionic liquids is desired. They have recently anticipated that ionic liquids containing alkylsulfonate or alkylsulfate anions are better options from an environmental perspective than ionic liquids containing anions with fluorine atoms, such as hexafluorophosphate or bis(trifluoromethanesulfonyl)amide ions [16].

The ILs with alkyl-substituted imidazolium cation and dialkylphosphate anions can be synthesized using a one-pot method with high yield, low cost and ease of purification [17–19]. Compared with the chloride-based ionic liquids, alkyl phosphate anions have sufficiently high hydrogen bond basicity and lower viscosities [20]. Especially, this kind of ILs with an inorganic ester group might exhibit a high affinity toward CO_2. To the best of our knowledge, CO_2 capture mechanisms in ILs with alkyl-substituted imidazolium cations and dialkylphosphate anions, has never been studied so far. In this work, CO_2 capture mechanisms of this kind of ILs deprived of fluorinated anions – *i.e.* [MMIM]DMP, [EMIM]DMP and [EMIM]DEP – were investigated using an ATR FT-IR spectroscopy method developed in prior studies [21,22]. In addition, the swelling behaviors of the three ILs as a result of CO_2 absorption were investigated.

2. Experimental

2.1. Materials

[MMIM]DMP, [EMIM]DMP and [EMIM]DEP with a purity of 98.0% were supplied by Fisher scientific Co., and were used without further purification. Prior to testing, the materials were degassed and dried under vacuum for 12 h at 353.15 K. A little weight difference was observed before and after pretreatment. Samples obtained after pretreatment were characterized by ^{1}H NMR and ^{13}C NMR spectra, and no extra peak was found. The structures of the ILs are shown in Table 1. High-purity anhydrous carbon dioxide with a purity of 99.999% was obtained from Tech Air Co.

2.2. Apparatus and procedure

2.2.1. Attenuated total reflectance (ATR) FT-IR spectroscopy

In order to measure the CO_2 capture capacity and swelling behaviors of the ILs, and then analyze the absorption mechanisms, a Fourier-transform infrared (FT-IR) spectrometer (Nicolet 6700, Thermo Fisher Scientific Inc.) equipped with a deuterated triglycine sulfate (DTGS) detector, an attenuated total reflectance (ATR) accessory topped with a high-pressure fluid cell (Golder Gate™ Supercritical Fluids analyzer, Specac Ltd. (UK)) and a PID temperature controller was used in this study.

2.2.2. Measurement of CO_2 capture capacity and thermally-induced swelling

The CO_2 capture capacity and thermally-induced swelling were measured as described in prior studies [21]. Typically, a small amount of sample was deposited onto the surface of the diamond crystal, which was then heated to the desired temperature. Then the sample cell was pressurized with CO_2. The spectra were collected in the range 4000 cm^{-1}–500 cm^{-1} from the acquisition of 32 scans, with a resolution of 2 cm^{-1}.

Table 1
Ionic liquids used in the current study.

Ionic liquid	Structure
1,3-Dimethylimidazolium dimethylphosphate ([MMIM]DMP)	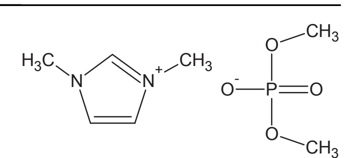
1-Ethyl-3-methylimidazolium dimethylphosphate ([EMIM]DMP)	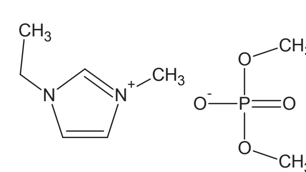
1-Ethyl-3-methylimidazolium 3-diethylphosphate ([EMIM]DEP)	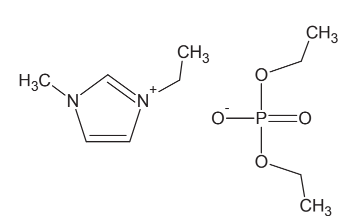

All samples reached equilibrium within 10 min, and the experiments were repeated at least twice under each temperature and pressure condition. The measurements were conducted from 0 to 4.83 MPa at either 298.15 K, 303.15 K or 313.15 K.

2.2.3. Measurement of CO_2 diffusivity

CO_2 diffusivity in ILs was also measured using ATR FT-IR spectroscopy equipped with a high pressure sample cell. Typically, a thin layer of sample was deposited on top of the diamond crystal. The temperature was set at 298.15 K and the thickness of the layer was measured using a caliper. The spectrum of the sample was then collected using the same acquisition parameters as described above. Afterwards, the sample cell was pressurized with CO_2 at 1.38 MPa. Spectra were then collected every 3 s up to reaching equilibrium. The CO_2 and IL absorbance bands were well resolved and did not require deconvolution techniques for spectral analysis. The CO_2 (2370–2310 cm^{-1}) absorbance band was integrated using a two-point base line correction.

3. Thermodynamic background

3.1. Calculation of CO_2 capture capacity and CO_2-induced swelling

The CO_2 capture capacities were determined from the ATR FT-IR spectroscopy measurements as described in prior studies [20]. Beer–Lambert law expresses the relationship between absorbance (A), absorptivity (ε), concentration (c), and effective thickness of the evanescent wave (d_e) [23]:

$$A = \varepsilon \cdot c \cdot d_e \tag{1}$$

The refractive index of ionic liquids ($n_{[MMIM]DMP} = 1.486$, $n_{[EMIM]DMP} = 1.483$ and $n_{[EMIM]DEP} = 1.475$) was used to calculate d_e as described in Ref. [23]. The absorbance of CO_2 was quantified by measuring the intensity of the stretching band around 2338 cm^{-1}. The molar absorptivity of CO_2 (ε) at high-pressure was considered equal to 1.0×10^6 cm^2/mol [24].

The degree of swelling (S) is defined as a ratio of the change of the solvent volume over the initial volume [25]:

$$S = \frac{A^0}{A} \cdot \frac{d_e}{d_e^0} - 1 \tag{2}$$

Sakellarios et al. already used this method to study the high-pressure CO_2-induced swelling of ILs [26]. Here, the absorbance of C-O stretching band around 1040 cm^{-1} from the ether groups of the ILs was used to calculate the swelling. This band was selected because it is relatively well-isolated from other bands and therefore does not require major deconvolution treatment. Because of the relative broad band of C-O, the swelling ratios obtained *via* the integration in the interval from 1075 cm^{-1} to 950 cm^{-1} would more likely represent the volume change of ILs. In this calculation, the absorptivity was assumed constant regardless of CO_2 concentration in the sample. The absorptivity is involved in the calculation of the effective thickness [25], and therefore it resulted that the effective thickness was considered constant in the pressure range studied. Combining Eqs. (1) and (2), the CO_2 capture capacity in moles of CO_2 per gram of absorbent (m) can be determined as follows:

$$m = \frac{c}{M \times \frac{\rho}{1+S}} \times 1000 \tag{3}$$

Through m obtained above, the CO_2 solubility in mole fraction basis (x) can be further calculated using the following equation:

$$x = \frac{m}{1000/M_{IL}} \tag{4}$$

3.2. Gas–liquid phase equilibrium

The condition for the phase equilibrium is satisfied when the fugacities of the gas component have equal values in both phases at a constant temperature and pressure:

$$f_1^g = f_1^l \tag{5}$$

Due to the negligible vapor pressure of ILs, the gas phase is assumed to be pure CO_2. The fugacity of the pure carbon dioxide in gas phase can be expressed as the product of the total pressure (P) and the fugacity coefficient (φ_1). Therefore, the gas–liquid equilibrium expression is as follows:

$$f_1^g = P\varphi_1 \tag{6}$$

The fugacity coefficient of CO_2, φ_1, in Eq. (6) can be calculated using Span–Wagner equation of state. In contrast to the gas-phase fugacities, liquid-phase fugacities depend slightly on the pressure at constant temperature (T) and pressure:

$$f_1^l(P) = f_1^l(P_2^s)\exp\int_{P_2^s}^{P} \overline{V}_1 (RT)^{-1} dP \tag{7}$$

The solubility data of CO_2 in ionic liquids can be correlated using the Krichevsky–Kasarnovsky (K–K) equation, which does not take into account the non-ideality of the solute in the liquid phase:

$$\ln\frac{f_1^l}{x_1} = \ln K_H^{P_2^s} + \frac{\overline{V}_1^{\infty}(P - P_2^s)}{RT} \tag{8}$$

Because the saturated vapor pressure of ionic liquid is negligible, it is reasonable to assume P_2^s to be zero. Therefore, Eq. (8) can be re-arranged as follows:

$$\ln\frac{f_1}{x_1} = \ln K_H^0 + \frac{\overline{V}_1^{\infty} P}{RT} \tag{9}$$

By plotting and fitting the natural logarithm of the ratio of fugacity to the solubility of CO_2 versus the CO_2 pressure, Henry's law constant (K_H^0) and the CO_2 partial molar volume ($\overline{V}_1^{\infty}$) at different temperatures can be obtained.

4. Results and discussions

4.1. Interactions of CO_2 with the ILs

Gurkan et al. reported that FT-IR spectroscopy can be used to distinguish the fractions of physically dissolved and chemically reacted CO_2 since the physically dissolved CO_2 appears cleanly between 2370 and 2310 cm^{-1} [27]. In this work, ATR FT-IR spectroscopy was used to obtain information about the interactions of CO_2 with [MMIM]DMP, [EMIM]DMP and [EMIM]DEP, which seem to be responsible for the enhanced solubility of CO_2 in phosphate-based ILs. Fig. 1(a) shows the ATR FT-IR spectra of CO_2 stretching band in [MMIM]DMP at various partial pressures of CO_2 ranging from 0 to 4.83 MPa, at 298.15 K. As CO_2 dissolved in the ILs, CO_2 stretching became more and more visible (~2338 cm^{-1}). The stretching of CO_2 progressively decreased in intensity and shifted as the pressure increased. This feature was observed by Kazarian et al. whose investigation showed that the anti-symmetric stretching mode of CO_2 dissolved in ionic liquids of [BMIM]PF_6 and [BMIM]BF_4 appears at about 2338 cm^{-1} [28–30]. CO_2 molecule also exhibits a FT-IR active bending mode, which usually appears around 670 cm^{-1}. When CO_2 is absorbed in a solvent, both the stretching mode and the bending mode could theoretically be observed. This has for instance been reported by Kazarian et al. who investigated CO_2 absorption in [BMIM]PF_6 and [BMIM]BF_4 [28]. In the present study, the absorbance strength related to CO_2 bending mode was very weak (Fig. 1(b)). This feature can be due to the fact that the groups of [MMIM]DMP, [EMIM]DMP and [EMIM]DEP strongly absorb in the region of the bending mode of CO_2, such as the P–O groups in the ILs (Fig. 1(b)).

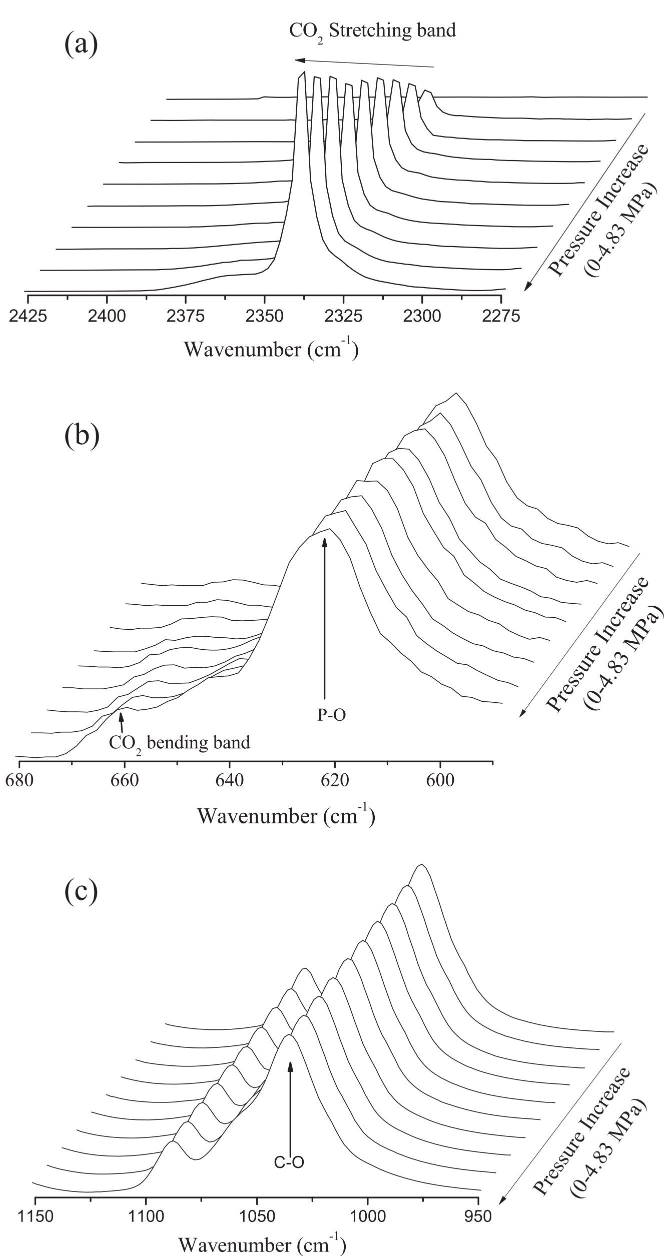

Fig. 1. ATR FT-IR spectra of [MMIM]DMP at 298.15 K under increasing CO_2 partial pressure (0–4.83 MPa): (a) CO_2 stretching band as a function of CO_2 pressure. (b) CO_2 bending band and P–O as a function of CO_2 pressure. (c) C–O as a function of CO_2 pressure.

4.2. Diffusivity of CO_2 in the ILs

The diffusivity of CO_2 in the ILs is crucial to both an understanding of the physical mechanisms controlling transport, as well as an ultimate prediction of the transport rate. The ATR FT-IR spectra of 500 scans for [MMIM]DMP, [EMIM]DMP and [EMIM]DEP at equilibrium were collected under the initial pressure of 1.38 MPa and 298.15 K. CO_2 diffusion coefficients, D_{CO_2}, were calculated by the following equation [31]:

$$\frac{A}{A_{eq}} = 1 - \frac{4}{\pi}\exp\left(\frac{-\pi^2 D_{CO_2} t}{4l^2}\right) \tag{10}$$

CO_2 diffusion coefficients in [MMIM]DMP, [EMIM]DMP and [EMIM]DEP under the initial pressure of 1.38 MPa at 298.15 K were 1.53×10^{-6} cm^2/s, 0.95×10^{-6} cm^2/s and 0.42×10^{-6} cm^2/s, respectively. This result indicated that the order of magnitude for the diffusion coefficient of CO_2 in ILs with phosphate-based anion is very close to the values reported for ILs with Tf_2N, PF_6, or BF_4 anion (10^{-6} cm^2/s) [32]. Fig. 2 illustrates the kinetics of CO_2 absorption in the three ILs at 1.38 MPa and 298.15 K. The absorption of CO_2 was complete in about 6 min for [EMIM]DEP, in 4 min for [EMIM]DMP, and in 3 min for [MMIM]DMP. This trend is likely related to the viscosities of the ILs which were 412 mPa s for [EMIM]DEP, 270 mPa s for [EMIM]DMP and 168 mPa s for [MMIM]DMP.

4.3. CO_2-induced swelling of ILs

The CO_2-induced swelling (S) of ILs at various temperatures and pressures is an important feature in the evaluation of ILs for use in industrial gas treating process. Fig. 1(c) shows ATR FT-IR spectra of C-O in [MMIM]DMP at 298.15 K and

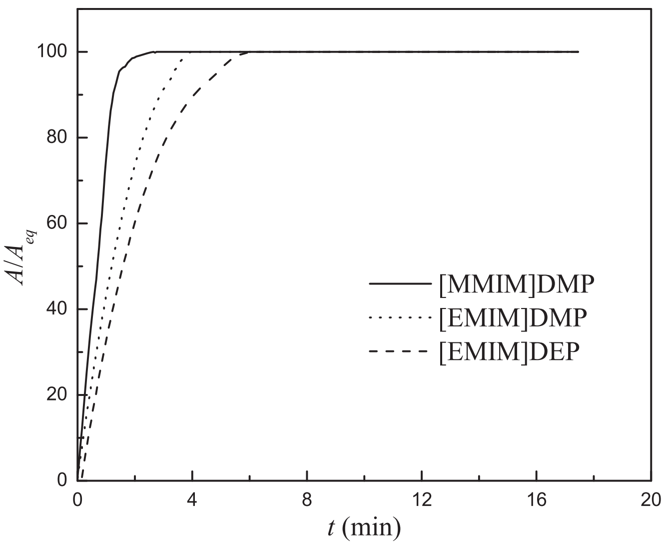

Fig. 2. CO_2 diffusion in the three ILs as a function of time at 1.38 MPa and 298.15 K. A/A_{eq} represents the ratio of the absorbance of CO_2 stretching band at any time over the absorbance of CO_2 stretching band at equilibrium.

under increasing CO_2 partial pressure (0–4.83 MPa). Using Eq. (2) along with the spectroscopic data before and after exposure to CO_2 in the interval from 950 cm^{-1} to 1075 cm^{-1} at different temperatures and pressures, the CO_2-induced swelling of the three ILs was calculated. The results are listed in Tables 2–4. With the increasing alkyl chain length of phosphate-base ionic liquid, swelling slightly increased. At the temperature of 298.15 K and the pressure of 4.83 MPa, the CO_2-induced swellings of [MMIM]DMP, [EMIM]DMP and [EMIM]DEP were 17.33%, 18.50% and 19.74%, respectively. This result may be attributed to the fact that more CO_2 was absorbed in ILs with the increase of alkyl chain length in anions or cations of ILs, as confirmed in the next section. Fig. 3 shows the extent of swelling for the [MMIM]DMP in the pressure range 0–4.83 MPa at different temperatures. As seen in Fig. 3, an increment in temperature resulted in the decreasing extent of swelling for the [MMIM]DMP mainly due to the decrease of CO_2 solubility. Also, absorption of CO_2 in the ILs led to an increase in the volume of the liquid phase. This increase in liquid volume could be attributed to the fact that compressed CO_2 reduced the surface tension of liquids,

Table 2
List of experimental ($x^{exp}_{CO_2}$) and calculated ($x^{cal}_{CO_2}$) solubilities of CO_2 in [MMIM]DMP, their associated CO_2-induced swelling (S%), relative deviations (RD) as well as experimental mass fraction ($w^{exp}_{CO_2}$) at different temperatures and pressures.

P (MPa)	$x^{exp}_{CO_2}(\times 100)$	$x^{cal}_{CO_2}(\times 100)$	RD	S (%)	$w^{exp}_{CO_2}$ ($\times 100$)
T = 298.15 K					
0.34	4.91	4.86	1.01	2.38	1.02
0.69	9.22	9.14	0.92	4.18	2.01
1.03	12.90	12.88	0.15	5.80	2.93
1.38	16.20	16.13	0.43	7.48	3.83
1.72	18.80	18.93	−0.71	8.72	4.59
2.07	21.12	21.33	−0.98	9.98	5.31
2.76	24.64	25.04	−1.62	12.06	6.48
3.45	27.12	27.53	−1.54	13.94	7.37
4.83	30.40	29.70	2.33	17.33	8.66
T = 303.15 K					
0.34	4.15	4.12	0.84	1.74	0.86
0.69	7.89	7.79	1.19	3.09	1.70
1.03	11.16	11.05	0.97	4.71	2.49
1.38	13.92	13.93	−0.07	5.90	3.21
1.72	16.29	16.46	−1.09	7.11	3.86
2.07	18.30	18.67	−2.04	8.35	4.44
2.76	21.92	22.23	−1.39	10.40	5.56
3.45	24.67	24.78	−0.45	11.99	6.49
4.83	28.01	27.48	−1.87	15.31	7.71
T = 313.15 K					
0.34	3.15	3.14	0.32	1.10	0.65
0.69	6.05	6.03	0.22	2.22	1.28
1.03	8.70	8.69	0.16	3.36	1.89
1.38	11.11	11.11	0.00	4.30	2.48
1.72	13.30	13.33	−0.26	5.25	3.04
2.07	15.29	15.35	−0.35	6.22	3.58
2.76	18.73	18.82	−0.48	7.71	4.57
3.45	21.63	21.63	0.01	9.24	5.47
4.83	25.64	25.52	0.46	12.44	6.83
ARD% = 0.81					

$RD = \frac{x^{cal}_{CO_2} - x^{exp}_{CO_2}}{x^{exp}_{CO_2}} \times 100 \quad w^{exp}_{CO_2} = \frac{m \times 44}{1000}$

Table 3
List of experimental ($x^{exp}_{CO_2}$) and calculated ($x^{cal}_{CO_2}$) solubilities of CO_2 in [EMIM]DMP, their associated CO_2-induced swelling (S%), relative deviations (RD) as well as experimental mass fraction ($w^{exp}_{CO_2}$) at different temperatures and pressures.

P (MPa)	$x^{exp}_{CO_2}(\times 100)$	$x^{cal}_{CO_2}(\times 100)$	RD	S (%)	$w^{exp}_{CO_2}$ ($\times 100$)
T = 298.15 K					
0.34	5.50	5.40	1.83	2.80	0.97
0.69	10.27	10.17	1.00	4.70	1.91
1.03	14.29	14.36	−0.45	6.40	2.78
1.38	17.96	18.02	−0.35	8.10	3.65
1.72	21.00	21.20	−0.97	9.30	4.43
2.07	23.67	23.94	−1.12	10.60	5.17
2.76	27.81	28.24	−1.55	12.80	6.42
3.45	31.12	31.19	−0.22	14.70	7.53
4.83	34.56	33.95	1.76	18.50	8.80
T = 303.15 K					
0.34	4.70	4.66	0.84	2.12	0.82
0.69	8.90	8.85	0.63	3.52	1.63
1.03	12.62	12.59	0.25	5.18	2.41
1.38	15.96	15.92	0.29	6.42	3.17
1.72	18.70	18.87	−0.86	7.68	3.83
2.07	21.27	21.46	−0.89	8.97	4.50
2.76	25.34	25.70	−1.43	11.11	5.66
3.45	28.75	28.83	−0.29	12.75	6.72
4.83	32.82	32.37	1.38	16.21	8.14
T = 313.15 K					
0.34	3.65	3.64	0.23	2.47	0.63
0.69	7.00	7.01	−0.14	3.65	1.25
1.03	10.16	10.13	0.32	4.63	1.89
1.38	12.98	13.01	−0.20	5.64	2.49
1.72	15.60	15.66	−0.41	6.66	3.08
2.07	18.03	18.09	−0.37	8.26	3.67
2.76	22.44	22.36	0.39	9.89	4.82
3.45	25.96	25.88	0.30	13.25	5.84
4.83	30.92	30.98	−0.18	14.86	7.46
ARD% = 0.69					

Table 4
List of experimental ($x_{CO_2}^{exp}$) and calculated ($x_{CO_2}^{cal}$) solubilities of CO_2 in [EMIM]DEP, their associated CO_2-induced swelling (S%), relative deviations (RD) as well as experimental mass fraction ($w_{CO_2}^{exp}$) at different temperatures and pressures.

P (MPa)	$x_{CO_2}^{exp}(\times 100)$	$x_{CO_2}^{cal}(\times 100)$	RD	S (%)	$w_{CO_2}^{exp}(\times 100)$
T = 298.15 K					
0.34	6.69	6.63	0.80	3.41	1.19
0.69	12.55	12.50	0.44	5.81	2.39
1.03	17.85	17.65	1.12	7.69	3.62
1.38	22.20	22.16	0.19	9.31	4.76
1.72	25.89	26.07	−0.69	10.64	5.82
2.07	29.07	29.44	−1.27	12.00	6.83
2.76	34.18	34.73	−1.61	14.47	8.66
3.45	37.93	38.38	−1.17	16.29	10.18
4.83	42.66	41.79	2.04	19.74	12.41
T = 303.15 K					
0.34	5.91	5.84	1.19	2.47	1.05
0.69	11.10	11.07	0.28	4.18	2.08
1.03	15.78	15.73	0.35	5.95	3.12
1.38	19.77	19.86	−0.47	7.47	4.11
1.72	23.44	23.51	−0.28	8.72	5.10
2.07	26.59	26.70	−0.41	10.00	6.04
2.76	31.39	31.89	−1.59	12.31	7.63
3.45	35.36	35.66	−0.85	14.37	9.12
4.83	40.48	39.81	1.66	17.61	11.34
T = 313.15 K					
0.34	4.75	4.75	0.07	1.37	0.83
0.69	9.15	9.10	0.51	2.77	1.68
1.03	13.07	13.08	−0.05	3.92	2.51
1.38	16.69	16.70	−0.08	5.10	3.34
1.72	19.90	19.99	−0.43	6.30	4.14
2.07	22.94	22.96	−0.11	7.23	4.96
2.76	27.99	28.05	−0.20	9.44	6.47
3.45	32.12	32.10	0.05	11.41	7.89
4.83	37.65	37.56	0.24	14.86	10.07
ARD% = 0.72					

which then resulted in a decrease in mixture solvent strength. This result indicates that CO_2 is an effective anti-solvent.

4.4. CO_2 capture capacity of ILs

CO_2 capture capacities of [MMIM]DMP, [EMIM]DMP and [EMIM]DEP were calculated using Eq. (3) and listed in Tables 2–4, respectively. As shown in Fig. 4, a comparison of CO_2 solubilities in [MMIM]DMP, [EMIM]DMP and [EMIM]DEP clearly shows that CO_2 capture capacity of these ILs followed the order of [EMIM]DEP > [EMIM]DMP > [MMIM]DMP. For instance, at a pressure of 4.83 MPa and a temperature of 298.15 K, the solubility increased from 0.30 mole fraction for [MMIM]DMP, to 0.35 mole fraction for [EMIM]DMP, to 0.41 mole fraction for [EMIM]DEP. Similar trends were observed at 303.15 K and 313.15 K. The CO_2 solubility in this kind of phosphate-based ILs increased with the increasing alkyl chain length in cation/anion of ILs. These results are supported by the work of Aki et al. who found that CO_2 solubility in [Tf_2N]-based ILs increased with an increase in the alkyl chain length from butyl to octyl [13]. Similarly, Shariati and Peters reported that the solubility of CO_2 in $[PF_6]^-$ based ILs increased when the alkyl chain length was increased from ethyl to hexyl [33].

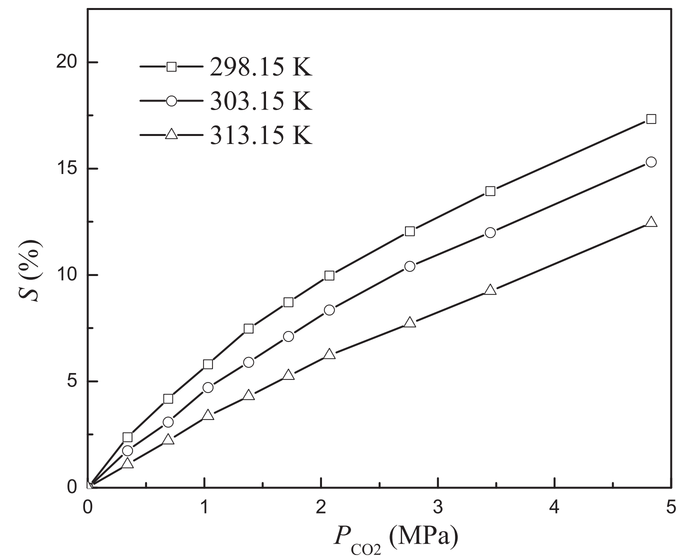

Fig. 3. CO_2-induced swelling (S%) of [MMIM]DMP as a function of pressure at different temperatures.

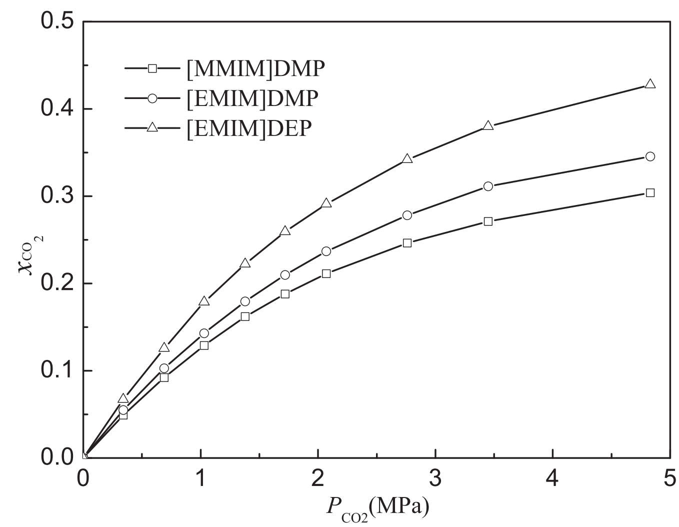

Fig. 4. CO_2 capture capacities of phosphate-based ILs (mole fraction of CO_2, x_{CO_2}) as a function of pressure at 298.15 K.

These results may be attributed to the fact that the densities of phosphate-based ILs decreased with the increase of alkyl chain length in IL. So [EMIM]DEP likely had more free volume which in turn allowed for more gas to dissolve. This result further indicates that physical absorption in the phosphate-based ionic liquids played a significant role for the solubility of CO_2.

4.5. Henry's law constants of CO_2 in phosphate-based ILs

The solubility data of CO_2 in ILs can be calculated using the Krichevsky–Kasarnovsky (K–K) and Span–Wagner equations [34], and the calculated results are listed in Tables 2–4. In Fig. 5, the logarithm of the ratio of fugacity to the

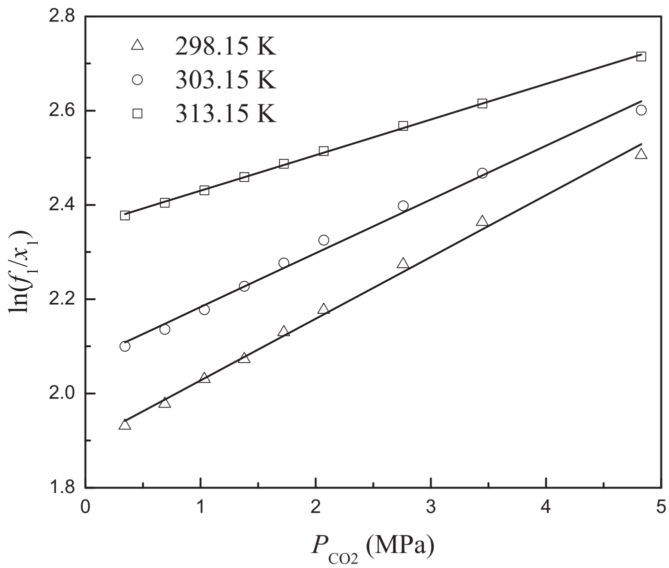

Fig. 5. K–K equation analysis of the solubilities of CO_2 in [MMIM]DMP. The lines represent the calculated values while the points correspond to the experimental data.

solubilities of CO_2 in [MMIM]DMP is plotted versus the pressure. Using this plot, the Henry's constants at zero pressure were obtained. The Henry's constants of [MMIM]DMP and [EMIM]DEP at 313.15 K were 10.54 MPa and 6.95 MPa, respectively, which are in good agreement with the values of 10.66 MPa and 6.94 MPa [35]. For [EMIM]DMP, the Henry's constant at the same conditions was 9.13 MPa, which was between the values of [MMIM]DMP and [EMIM]DEP. The Henry's constants of other ionic liquids with the same $[EMIM]^+$ cation as well as that of [BMIM]PF_6 have already been reported [36]. The Henry's constants at 298.15 K followed this order: [EMIM]Tf_2N < [EMIM]DEP < [BMIM]PF_6 < [EMIM]DMP <[EMIM]TfO < [EMIM]DCA < [EMIM] BF_4 (as shown in Fig. 6). The larger CO_2 solubility of [EMIM] DEP compared to the other two ILs suggests that ester-

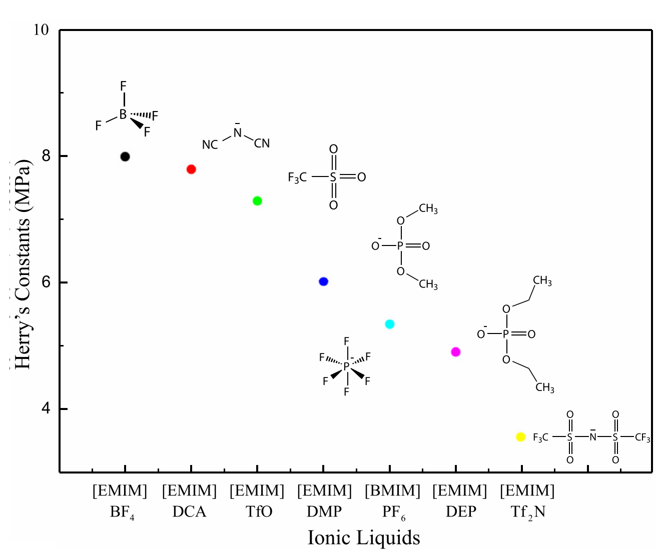

Fig. 6. Henry's constants of CO_2 in different ILs with the same cation except for [BMIM]PF_6 at 298.15 K.

containing anions may be advantageous to CO_2 capture and/or that phosphate-containing anions (like DEP and DMP) may favor CO_2 capture.

5. Conclusions

In this study, ATR FT-IR spectroscopy was used to determine the CO_2 capture capacity and CO_2-induced swelling of phosphate-based ionic liquids over the temperature range from 298.15 to 313.15 K and pressures up to 4.83 MPa. CO_2 capture mechanism in the three ILs studied in this work was determined as physical absorption. With the increase of the alkyl chain length in ILs, the free volume of ILs increased, which caused the CO_2 solubility to increase and the diffusion coefficient to decrease. Over the temperature range from 298.15 to 313.15 K, Henry's law constants of CO_2 in [MMIM]DMP ranged from 6.66 to 10.54 MPa, those in [EMIM]DMP ranged from 6.02 to 9.13 MPa, and those in [EMIM]DEP ranged from 4.90 to 6.95 MPa, following an inverse relationship with solubility.

Conflict of interest

The authors declared that they have no conflicts of interest to this work.

Acknowledgements

This work was supported by the National Natural Science Foundation of China (21206165 and U1407111).

Symbols used

A^0	absorbance without CO_2 pressure
A	absorbance with CO_2 pressure
c	concentration (g cm^{-3})
d_e	arithmetical mean between the effective path length for perpendicular and parallel polarization
d_e^0	effective path length without CO_2 pressure
D_{CO_2}	diffusion coefficient of CO_2 in ionic liquids
f_1	fugacity of CO_2 in the gas phase at system temperature and pressure
f_1^g	fugacity of carbon dioxide in gas phase
f_1^l	fugacity of carbon dioxide in liquid phase
$K_H^{P_2^s}$	Henry's law constant on mole-fraction scale of CO_2 in ionic liquid at saturated vapor pressure of ionic liquid
K_H^0	Henry's law constant at zero pressure
l	the thick of ionic liquid film (mm)
m	CO_2 capture capacity (mol kg^{-1})
M	molecular weight of CO_2 (g mol^{-1})
M_{IL}	molecular weight of ionic liquid (g mol^{-1})
P	total pressure P (MPa)
P_2^s	saturated vapor pressure of ionic liquid
R	universal gas constant

S degree of swelling
t time (s)
T temperature (K)
$\overline{V}_1$ the partial molar volume of CO_2 in ionic liquid (m^3 mol^{-1})
$\overline{V}_1^{\infty}$ partial molar volume of CO_2 at dilution condition in liquid phase (m^3 mol^{-1})
x_i^{cal} calculated mole fraction
$x_i^{\exp}$ experimental mole fraction
ρ density (g cm^{-3})
φ_1 fugacity coefficient
ε a constant related to the optical properties of the absorbing substance (1.0×10^6 cm^2 mol^{-1})

References

[1] R.E. Baltus, R.M. Counce, B.H. Culbertson, H. Luo, D.W. DePaoli, S. Dai, D.C. Duckworth, Sep. Sci. Technol. 40 (2005) 525–541.
[2] A.B. Rao, E.A. Rubin, Environ. Sci. Technol. 36 (2002) 4467–4475.
[3] P.G. Jessop, R.R. Stanley, R.A. Brown, C.A. Eckert, C.L. Liotta, T.T. Ngo, P. Pollet, Green Chem. 5 (2003) 123–128.
[4] H. Kawanami, A. Sasaki, K. Matsui, Y. Ikushima, Chem. Commun. (2003) 896–897.
[5] K.R. Seddon, A. Stark, M.J. Torres, Pure Appl. Chem. 72 (2000) 2275–2287.
[6] F. Heym, J. Haber, W. Korth, B.J.M. Etzold, A. Jess, Chem. Eng. Technol. 33 (10) (2010) 1625–1634.
[7] R. Fortunato, C.A.M. Afonso, A.M. Reis, J.G. Crespo, J. Membr. Sci. 242 (2004) 197–209.
[8] J.F. Brennecke, B.E. Gurkan, J. Phys. Chem. Lett. 1 (2010) 3459–3464.
[9] C. Cadena, J.L. Anthony, J.K. Shah, T.I. Morrow, J.F. Brennecke, E.J. Maginn, J. Am. Chem. Soc. 126 (2004) 5300–5308.
[10] J.L. Anthony, J.L. Anderson, E.J. Maginn, J.F. Brennecke, J. Phys. Chem. B 109 (2005) 6366–6374.
[11] S.N.V.-K. Aki, B.R. Mellein, E.M. Saurer, J.F. Brennecke, J. Phys. Chem. B 108 (2004) 20355–20365.
[12] J. Völkl, K. Müller, L. Mokroshina, W. Arlt, Chem. Eng. Technol. 35 (3) (2012) 579–583.
[13] J. Lu, C.L. Liotta, C.A. Eckert, J. Phys. Chem. A 107 (2003) 3995–4000.
[14] H. Liu, H. Tian, H. Yao, D. Yu, W. Zhao, X. Bai, J. Phys. Chem. A 36 (8) (2013) 1402–1410.
[15] J.H. Huang, T. Rühter, Aust. J. Chem. 62 (2009) 298–308.
[16] P. Wasserscheid, R. van Hal, A. Bosmann, J. Esser, A. Jess, In Ionic Liquids as Green Solvents: Progress and Prospects, Oxford University Press, New York, 2003, p. 57.
[17] J.D. Holbrey, W.M. Reichert, R.P. Swatloski, G.A. Broker, W.R. Pitner, K.R. Seddon, R.D. Rogers, Green Chem. 4 (2002) 407–413.
[18] J.F. Wang, C.X. Li, Z.H. Wang, Z.J. Li, Y.B. Jiang, Fluid Phase Equilib. 255 (2007) 186–192.
[19] J.F. Wang, Z.B. Li, J. Chem. Eng. Data 58 (2013) 1641–1649.
[20] Y. Hiraga, M. Goto, Y. Sato, R.L. Smith, J. Chem. Thermodyn. 104 (2017) 73–81.
[21] K.-Y.A. Lin, A.-H.A. Park, Environ. Sci. Technol. 45 (2011) 6633–6639.
[22] Y.J. Park, J. Decatur, K.-Y.A. Lin, A.-H.A. Park, Phys. Chem. Chem. Phys. 13 (2011) 18115.
[23] N.J. Harrick, Internal Reflection Spectroscopy, Interscience Publishers, New York, NY, 1967.
[24] P.G. Maiella, J.W. Schoppelrei, T.B. Brill, Appl. Spectrosc. 53 (1999) 351–355.
[25] I. Pasquali, J.-M. Andanson, S.G. Kazarian, R. Bettini, J. Supercrit. Fluids 45 (2008) 384–390.
[26] N.I. Sakellarios, S.G. Kazarian, ACS Symp. Ser. 901 (2005) 89.
[27] B.E. Gurkan, J.C. de la Fuente, E.M. Mindrup, L.E. Ficke, B.F. Goodrich, E.A. Price, W.F. Schneider, J.F. Brennecke, J. Am. Chem. Soc. 132 (2010) 2116–2117.
[28] S.G. Kazarian, B.J. Briscoe, T. Welton, Chem. Commun. (2000) 2047–2048.
[29] J.L. Anthony, E.J. Maginn, J.F. Brennecke, J. Phys. Chem. B 106 (2002) 7315–7320.
[30] L.A. Blanchard, Z.Y. Gu, J.F. Brennecke, J. Phys. Chem. B 105 (2001) 2437–2444.
[31] K.C. Farinas, L. Doh, S. Venkatraman, R.O. Potts, Macromolecules 27 (1994) 5220–5222.
[32] Y. Hou, R.E. Baltus, Ind. Eng. Chem. Res. 46 (2007) 8166–8175.
[33] A. Shariati, C.J. Peters, J. Supercrit. Fluids 29 (2004) 43–48.
[34] R. Span, W.J. Wagner, Phys. Chem. Ref. Data 25 (1996) 1509–1596.
[35] J. Palgunadi, J.E. Kang, M. Cheong, H. Kim, H. Lee, H.S. Kim, Bull. Korean Chem. Soc. 30 (2009) 1749–1754.
[36] F. Karadas, M. Atilhan, S. Aparicio, Energy Fuels 24 (2010) 5817–5828.